

Numerical and Experimental Investigations of Welded Butt Joints of (AISI304)

Dr. Muna. K. Abbass* , Dr.Karima E. Amori^{id}
& Rashaq A.Mohammed*

Received on: 27/1/2009

Accepted on: 5/11/2009

Abstract

Simulation of welding process (TIG or GTAW) of butt joint using finite element analysis is presented. The base metal is ST(304). The numerical model developed by include moving heat source, temperature dependent material properties, phase change and transformation, and mechanical analysis. The parameters studied numerically were welding current ranging between (80-150A) depending on, welding velocity, plate thickness (2.5mm -5mm), and material of the heat sink (carbon steel and copper). The numerical results show that increasing the welding current with increasing of welding speed decreases the fusion zone area. Using copper plate underneath the welded plates acts as a dissipation heat sink which generates stronger heat gradient compared with carbon steel plate. The experimental results show that increasing welding current leads to increasing the micro hardness, and the microstructure becomes smaller. Due to increasing cooling rate the microhardness have maximum value at the boundary between the Fusion zone and heat affected zone.

Keywords: welding simulations, heat transfer in welding, numerical heat transfer of welding

دراسة نظرية وعملية لوصلات اللحام المتقابلة لمادة (AISI304)

الخلاصة

تمت محاكاة عملية اللحام بطريقة (قطب التنجستن المحمي بالغاز) او (لحام القوس الكهربائي المحمي بالغاز) لوصلة لحام متقابلة بطريقة العناصر المحددة . كان المعدن الاساس هو فولاذ مقاوم للصداء (304) . بني النموذج العددي اعتمادا على مصدر حراري متحرك ؛ مادة متغيرة المواصفات مع درجة الحرارة ؛ انتقال حرارة غير مستقر لمادة متغيرة الطور، ولتحليل ميكانيكي. المتغيرات المدروسة عدديا كانت تيار اللحام (تراوح بين 80 الى 150 امبير) اعتمادا على سمك الصفيحة الملحومة ؛ سرعة اللحام ؛ وتأثير مادة الصفيحة الخلفية التي توضع عليها وصلة اللحام (فولاذ كاربوني او نحاس). تم التوصل عدديا الى قيم التوزيع الزمني لدرجات الحرارة بالاتجاه الأفقي والعمودي . بينت النتائج العددية ان زيادة تيار اللحام يؤدي الى تقليل حجم منطقة الأنصهار. أن استخدام صفيحة نحاس تحت القطع الملحومة عملت كمصب حراري جيد لنقل الحرارة من الوصلة الملحومة مقارنة باستخدام قطعة من الفولاذ الكاربوني. أظهرت النتائج العملية ان زيادة تيار اللحام يؤدي الى زيادة الصلابة الدقيقة وصغر البنية المجهرية. تم التوصل عمليا أن زيادة معدل التبريد أدت الى جعل القيم العظمى للبنية المجهرية تتواجد على الحد الفاصل بين منطقة الأنصهار والمنطقة المتأثرة بالحرارة.

Introduction

Fusion welding is a metallurgical fusion process in which parts or work pieces are joined by heating their connecting edges above their melting temperature and then solidified [1]. There are many types of the welding defects to result in the fusion zone and heat affected zone such as: microstructure defects in fusion and heat affected zone, hot and cold cracking in weld, the deformation due to welding and residual stresses. All these defects are created during or after welding. Hence the study of heat input and heat transfer in welding is very important to identify these defects. Welding simulation predicts welding deformations and stresses in the design requirements, reducing the extent of experimental tests and accelerating optimizations[2]. **Hsu and Rubinsky (1988)** [3], expressed a two-dimensional, quasi-stationary finite element numerical model to study the fluid flow and heat transfer phenomena which occur during constant travel speed, keyhole plasma arc used for welding of metal plate. The results show that the method can predict the shape of the welding pool as a function of welding parameters and that the widths of both the fusion zone and the heat affected zone are decreased as the welding speed increases while the power required for welding increases with an increase in welding speed **Justin Francis (2002)**[4], simulated the welding of the butt and tee joints (GMAW) using the software SYSWELD+®, based on finite element method for the quasi-steady state analysis. The base metal is aluminum alloy 2519-T87 and the filler material is alloy 2319. The results show that the maximum

residual longitudinal normal stress was within 3.6% of published data, while for a fully transient analysis this maximum stress was within 13%.

Mads Martinussen (2007)[5], studied numerically the robotic welding by spot (TIG) process using a software environment based on the finite element method, the model adopted is applied to trajectory planning and speed control of the welding robot to achieve better quality welds in an automated system.

The scope of present work is divided into two parts: Study experimentally the (welding current, welding voltage, welding speed, and welding time period) effect for stainless steel plate by (TIG) welding process as a butt joint with different plate thickness. These parameters are used as input data to the computational model utilizing finite element method to develop a Fortran computer program for transient thermal analysis of the welding process to compute the temperature distribution, which is important for cooling rate and heat gradient calculations.

Mathematical Model

Conservation of Energy:-

The energy equation for an isotropic material is used to describe the weld thermal history [6].

$$\frac{\partial^2 T}{\partial x^2} + \frac{\partial^2 T}{\partial y^2} + \frac{\partial^2 T}{\partial z^2} + \frac{q \cdot}{k} = \frac{1}{a} \frac{\partial T}{\partial t} \quad \dots(1)$$

Where

a is the thermal diffusivity of the metal at time t

$q \cdot$ is the internal heat source per unite volume.

k thermal conductivity of the metal.

Initial and Boundary Conditions:-

The welded plate metal initial temperature is assumed uniform and equal to T_o , i.e.

$$T_{(x,y,0)} = T_o \quad \dots\dots(2)$$

The convective boundary condition on the upper surface of the welded plate (which in contact with ambient air) can be formulated using Newton's law of cooling, which is

$$q_{conv} = hA(T - T_\infty) \quad \dots\dots(3)$$

Due to the symmetry between right and left half of the welded plates, the right half will be considered in the numerical investigation. Hence the plate plane of symmetry and the plate edge are considered insulated faces as shown in Figure (1) i.e,

$$k \frac{\partial T}{\partial x_i} = 0 \quad i = 1,2 \quad \dots\dots(4)$$

Where i refers to X and Y coordinates.

Since the welded plate is placed on a table, hence the conductive heat transfer from the plate to the table across the lower plate surface can be rewritten as:

$$k = \frac{\partial T_1}{\partial y} \Big|_{plate} = k' \frac{\partial T_2}{\partial y} \Big|_{table} \quad \dots\dots(5)$$

Where k' is thermal conductivity of table metal and subscripts 1 & 2 refer to plate and table respectively.

Finally the welding surface exposed to specified heat flux q_s can be formulated mathematically across the central segment of the upper surface shown in fig.(1) as:

$$k = \frac{\partial T_1}{\partial y} \Big|_{plate} = q_s \quad \dots\dots(6)$$

Convective Heat transfer Coefficient:-

Simplified equation for the coefficient of convective heat transfer from the upper surface of welded plate exposed to air at T_∞ is given by [6] (based on natural convection).

$$h = 0.59 \left(\frac{\Delta T}{L} \right)^{\frac{1}{4}} \quad \dots\dots(7)$$

Where h = heat transfer coefficient, $W/m^2 \cdot ^\circ C$ $\Delta T = T - T_\infty, ^\circ C$,

L = surface length that exposed to air, m

Solidification Equilibrium:-

For equilibrium solidification, the solid fraction f_s is related to the temperature by

$$f_s = \frac{1}{1 - K_o} \left\langle \frac{T - T_L}{T - T_f} \right\rangle \quad \dots\dots(8)$$

where T_L is the liquidus temperature, T_f is the solidus temperature of the pure material and K_o is a constant. Scheil Equation relating the solid fraction to temperature as: [3]

$$f_s = 1 - \left[\frac{T_f - T}{T_f - T_l} \right]^{\frac{1}{(K_o - 1)}} \quad \dots\dots(9)$$

For linear relationship the value $1/(K_o - 1)$ is equal to (1) and the liquid fraction f_l can be written as

$$f_l = \left[\frac{T_f - T}{T_f - T_l} \right] \quad \dots\dots(10)$$

Heat Input and Arc Efficiency Factor

The heat-input (Q) is one of the parameters that affect the temperature value. This can be interpreted as the net heat input or energy applied. In

general the heat input is defined as follows [5].

$$Q = \left(\frac{E.I.60}{V.1000} \right) \times \eta \quad \dots(11)$$

Where:

I = welding current (Ampere),

E=welding voltage (Volt)

η = arc efficiency factor,

V =The welding speed [mm/min]

NUMERICAL ANALYSIS

Finite Element Method (FEM)

Formulation:-

The unknown temperature T is approximated in the elemental solution domain at any time by:

$$T = \sum_{i=1}^n N_i T_i(t) \quad \dots(12)$$

Where T_i is the instantaneous temperature value of node i , and n is the number of elemental nodes (4 noded quadrilateral elements used in this work), and N_i is a linear interpolation functions. Discretization of equation (1) is adopted with FEM to give elemental matrices and vector. The assembly of these elemental matrices into global matrices and vector give first order transient simultaneous differential equations of the form [7, 8]:

$$C\dot{T} + KT = F$$

The elemental matrices and vector can be computed from:

$$C_{ij}^e = \int_{\Omega^e} \rho c N_i N_j d\Omega \quad \dots (13)$$

$$K_{ij}^e = \int_{\Omega} \left(k \frac{\partial N_i}{\partial x} \frac{\partial N_j}{\partial x} + k \frac{\partial N_i}{\partial y} \frac{\partial N_j}{\partial y} \right) d\Omega + \int_s h N_i N_j d\Gamma \quad \dots(14)$$

$$F_i^e = \int_{s^e} N_i h T_{\infty} d\Gamma \quad \dots(15)$$

Grid Generation:-

The physical domain is divided into sub divisions 540 (quadrilateral 4 noded linear elements) and 610 nodes including the work pieces and the back up metal as shown in Fig.(2).

Transient Solution by Θ -Method

The procedure relies on deriving recursion formulas relate the values of $\{T\}$ at one instant of time t to the values of $\{T\}$ at a later time $t + \Delta t$. The recursion formulas make it possible for the solution to be ‘marched’ in time, starting from the initial conditions at time $t=0$ and continuing step by step until reaching the desired duration. Denote a typical time in the response such that $\{t\}$.

$$t^n = t^o + \Delta t$$

Where superscripts (n, o) refer to new and old respectively. A general family algorithms result by introducing a parameter Θ such that:-

$$[C] \left\{ \dot{T} \right\}_{\Theta} + [K] \{T\}_{\Theta} = \{F\}_{\Theta} \quad \dots(16)$$

Where $0 \leq \Theta \leq 1$

Introducing the approximations:

$$\left\{ \dot{T} \right\}_{\Theta} = \frac{\{T\}^n - \{T\}^o}{\Delta t} \quad \dots(17)$$

$$\{T\}_{\Theta} = (1-\Theta)\{T\}^o + \Theta\{T\}^n \quad \dots(18a)$$

$$\{F\}_{\Theta} = (1-\Theta)\{F\}^o + \Theta\{F\}^n \quad \dots(18b)$$

Substituting equation (17) and (18) into equation (16) yields:

$$\left[\Theta[K] + \frac{1}{\Delta t}[C] \right] \{T\}^n = \left[-(1-\Theta)[K] + \frac{1}{\Delta t}[C] \right] \{T\}^o + (1-\Theta)\{F\}^o + \Theta\{F^n\} \quad \dots (19)$$

Here the vector $\{T\}^n$ on this L.H.S of this equation are unknowns, and all of the terms on the R.H.S are known. Equation (19) represents a general family of recurrence relation. The value of Θ is taken as (2/3) by adopting Galerkin method to ensure stable and converged solution. Equation (19) becomes[8]:

$$\left[\frac{2}{3}[K] + \frac{1}{\Delta t}[C] \right] \{T\}^n = \left[\frac{-1}{3}[K] + \frac{1}{\Delta t}[C] \right] \{T\}^o + \frac{1}{3}\{F\}^o + \frac{2}{3}\{F^n\} \quad \dots(20)$$

This equation can be rewritten in matrix form:

$$AX = B \quad \dots(21)$$

Where

$$A = \left[\frac{2}{3}[K] + \frac{1}{\Delta t}[C] \right]$$

$$X = \{T\}^n$$

$$B = \left[\frac{-1}{3}[K] + \frac{1}{\Delta t}[C] \right] \{T\}^o + \frac{1}{3}\{F\}^o + \frac{2}{3}\{F^n\}$$

equation 21 is solved by Gauss elimination method to compute the nodal temperature history. The numerical algorithm adopted in this work is transformed to a Fortran 90 computer program, the general flow chart is shown in the appendix.

EXPERIMENTAL WORK

The Used Materials

The used materials in TIG welding was stainless steel AISI(304) [9] which is shown in table (1), Physical Properties of Stainless Steel 304 shown in Table (2), and Mechanical Properties of stainless steel 304 are

shown in Table (3). Because the austenitic stainless steel are widely used in chemical, pharmaceutical, food industries, nuclear plants, and power generation industries. The work pieces of (2.5mm and 5mm) thickness have welded by TIG process.

Welding Process

Welding process of austenitic stainless steel (AISI304) was carried out by Tungsten Inert Gas Welding (TIG) or (GTAW). The welding electrodes type (E308) tungsten electrode type (Ewth-2) of (2.2 mm) diameter. Welding process was carried out with one pass in weld for each thickness (2.5mm and 5mm) voltage (32) volt, polarity (DCRP), and argon gas (99.1% Ar) at pressure (600 Kg/cm²) were remain constant. The TIG welding was achieved manually with the welder maintaining control over the arc length and directing the arc into the weld joint. The welding parameters used in this work are shown in Table (4).

Micro Hardness Test

The microhardness measurements were carried out along the cross section of welded sample in three zones the weld metal zone (WM), heat affected zone (HAZ), and the base metal zone (BM),for one side of weld and at distance of (1mm) between one reading and other.

RESULTS AND DISCUSSION

Numerical Results

The numerical results were carried out for three cases named.

Case one: Welding of (st.st304) plates of (2.5mm), placed on a table manufactured from carbon steel using three values of current (80, 90 and 100 A).

Case two: Welding of (st.st304) plates of (5mm) placed on carbon

steel table and three currents applied (130,140 and 150 A).

Case three: As in case two but the plates to be welded are placed on copper sheet of (2mm) thickness over the carbon steel table

Effect of Welding Current on The Temperature Distribution

Case one.

Figures (3a), (4a) and (5a) show the computational temperature contours within the welded joint (taken right half due to symmetry) for case one and for different welding current. The values of temperature distribution increases with increasing the welding current, where the peak temperature indicated within fusion zone were (1945°C, 2017°C and 2078°C) at time (1.7, 1.6, and 1.5 s from starting welding process) respectively for welding current (80, 90 and 100 A). Increasing the welding current leads to increase the power supply then increasing the temperature values as indicated in Figure (12). The metal is melted faster and cooled faster also the solidification process starts faster for (100A) compared with (80 A).

Figure (3b), (4b) and (5b) show the temperature distribution at time (2.2, 2.1, and 2 s from starting welding process) respectively, where temperature values reached (1363°C, 1479°C, and 1494°C).

Figure (3c), (4c) and (5c) show the temperature contours within the plate at time (3.2, 3.1, and 3 s) while Figures (3d), (4d) and (5d) show the temperature contours at time (5 s) where plate becomes colder.

Case Two

Figures (6a), (7a) and (8 a) show the computational temperature contours for the 5mm plates thickness subjected to welding current (130,

140 and 150 A) respectively at time (2.1, 2, and 1.9 s from starting welding process). Figure (13) shows the temperature history at welded joint surface (at plane of symmetry) for this case, the peak temperature indicated within fusion zone were (1952°C, 1960°C and 1981°C). The same trend as in case one is repeated here with noting that the solidification process starts for (150A) faster than that for (130A), since the welding period for (150A) was (1.9 s) while that for (130A) was (2.1 s).

Figures (6b), (7b) and (8b) present the thermal distribution within the welded joint at time (2.7, 2.6, and 2.5 s) for (130, 140 and 150 A) respectively, where maximum temperatures reached were (1640°C, 1631°C, and 1622°C).

Figure (6c), (7c) and (8c) show the temperature contours within the plate at time (3.7, 3.6, and 3.5 s) while Figures (6d), (7d) and (8d) show the temperature contours at time (5s) where plate becomes colder.

Case Three:-

In this case the behavior of the temperature distribution is in the same trend of case two but differs in values. Figures (9a, 10a, and 11a) show that the temperature values in welded joint at time (2.3,2.2, and 2.1 s) of the welded current (130,140, and 150 A) were (2025°C, 2064°C, and 2078°C) respectively, Figures (9b, 10b, and 11b) present temperature distribution at (2.8,2.7, and 2.6 s) where the temperature values are between (1788°C and 2002°C) for (130A) and (1788°C and 1945°C) for (140A) and (1631°C and 1788°C) for (150A) respectively. Figures (9c-d), (10c-d) and (11c-d) show the temperature distribution for

the three current values where the area of heat effected zone and temperature of it decreases with increase of welding current.

Generally, it could be seen that as welding current increases, the range of temperature distribution is increased, area of fusion zone decreases, and the area of heat affected zone decreases.

History of Temperature

Figures (12), (13), and (14) show the history of temperature within the plate for cases (one, two, and three) respectively. They indicate the temperature of the node belongs to the plate surface at the plane of symmetry of the welding joint. It rises rapidly when exposed to the welding arc heat flux. This temperature passes the melting temperature of the material which is defined as (1430°C - 1460°C). Solidification process is demonstrated and the material is cooled to approximately (600°C) within (10s) for cases one and two while for case three it reaches to (600°C) within m (6s) since in this case the copper plate behaves as a good heat sink for the welded parts.

The Experimental Results

The microhardness was measured by Vickers hardness tester along the cross-section of welded specimen in the three zones, weld metal (W.M), heat affected zone (HAZ), and base metal (B.M). Figures (15), (16),(17) show the microhardness of the three cases where it reaches value in the fusion zone area, and it increases when moving from the fusion zone center to the end of it along X-direction, the maximum value found was in the end of fusion zone at the boundary between the fusion zone and heat affected zone.

Microhardness is increased when welding current and thickness of work pieces increased. The effect of using the backing copper plate is clear where the value of it increases when you compare between the same current values of cases two and three, the copper plate is used to increase the cooling rate that leads to increasing the δ -ferrite. The high hardness in weld zone is due to presence of ($Cr_{23}C_6$) carbides and formulation of δ -ferrite.

Conclusions

From the results obtained for the computational and experimental work. It can be concluded that.

1-When the welding current increases the heat input is increased and the fusion zone area is decreased.

2-The micro hardness increases in the fusion zone area with welding current, and its value is increases towards the boundary of this zone reaching to the maximum value at the boundary between the fusion zone and heat affected zone.

3-The micro hardness value is increased at any point of the fusion zone with increasing the welding current.

References

- [1]Amstead,B.H.,Ostwald,P.F.and Beqeman,M. L. "Manufacturing Process",7th Ed. John Wiley, (1984)
- [2]Tashiro,Taka&Ushio "Numerical simulation of gas tungsten arc welding in different gases atmosphere", J. of Transaction of JWRI, Vol 34, pp.1567-1573, (2005)
- [3]Hsu,Y.F,and Rubinsky,B."Two-dimensional heat transfer study on the key hole plasma arc welding process". J. heat mass transfer V.31, pp.1409-1421, (1988).
- [4]Francis,J.D."Welding Simulation Of Aluminum Alloy Joints By FE

Analysis", M-Sc thesis, Aerospace Eng., Virginia Stat University, (2002)
 [5]Mads,Martnussen"Numerical Modeling And Model Reducation Of Heat Flow In Robitic Welding" MSc-thesis, Norwegian Univ.of Science & Technology, (2007).
 [6]Holman,J.P."Heat Transfer" Mc GRAW, Hill.INC., Eighth Edition,(1997).
 [7] Rao, S., S., (1982)," The Finite Element Method in

Engineering",PERGAMON PRESS, 1982.
 [8]Smith,I.M.and Griffiths, D.V. "Programming the Finite Element Method", John Wiley, Inc, (1998)
 [9]American Welding Society "Specification For Bare Stainless Steel Welding Electrodes And Rods",(1999)
 [10]Rany Alinberg.,Norman R.Braton "Welding And Other Joining Process" Ally and Bacon, Inc, Boston London , (1976).

<u>Symbol</u>	<u>Description</u>	<u>Units</u>
A	Area	[m ²]
[B]	Temperature-gradient interpolation matrix	[-]
[C]	Capacitance matrix	[-]
c _p	Specific heat	[kJ/kg K]
e	Element	[-]
{F}	Convective Vector	[-]
h	Convection heat transfer coefficient	[W/m ² .K]
[K]	Overall thermal stiffness matrix	[-]
k	Thermal conductivity	[W/m. °C]
L	Length	[m]
N _i	Interpolation function	[-]
n	Number of nodes	[-]
Q	heat input	[kJ/mm]
n	Number of element nodes	[-]
T	Temperature	[°C, K]
t	Time	[s]
v	Welding Velocity	[mm/min]
x, y, z	Cartesian coordinates	[m]
<u>Greek symbols</u>		
α	Thermal diffusivity	[m ² /s]
Θ	Dimensionless temperature	[-]
ρ	Density	[kg/m ³]
τ	Thermal stress	[N/m ²]; [-]
∇	Gradient operator	[-]
Ω	Domain boundary	[-]

Table (1) Chemical composition of stainless steel 304 [9]

Element	C%	Cr%	Ni%	Mn%	Si%	P%	S%	Rem
Wt%	0.08	18-20	8-10	2	1	0.03	.003	Fe

Table (2) Physical Properties of Stainless Steel 304 [9]

Property	Unit	Value
Density of solid metal	Kg/m ³	7800
Density of liquid metal	Kg/m ³	7200
Solidus temperature	°C	1430
Melting temperature	°C	1460
Specific heat of solid	J/g °C	1198
Specific heat of liquid	J/g °C	1254
Effective thermal conductivity of liquid	W/m.°C	209
Thermal conductivity of solid	W/m.°C	19

Table (3) Mechanical Properties of Stainless Steel 304[8]

Property	nit	Value
Yield Strength,	Pa	205
Ultimate Tensile Strength	Pa	515
Percent Elongation in 2 in. or 51 mm	C	40
Modulus of Elasticity	Pa	200

Table (4) The Welding Parameter Was Used in This Work

Sample Number	Base Metal	Thickness of plate(mm)	Electrode diameter (mm)	Welding current (A)
1	st.st 304	2.5	2	81
2	st.st 304	2.5	2	90
3	st.st 304	2.5	2	100
4	st.st 304	5	2.75	132
5	st.st 304	5	2.75	141
6	st.st 304	5	2.75	150
7	st.st 304	5	2.75	132
8	st.st 304	5	2.75	141
9	st.st 304	5	2.75	150

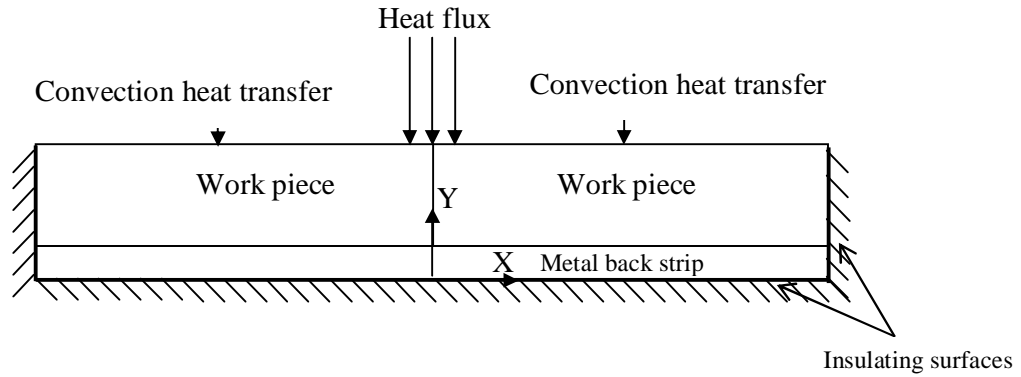


Figure (1) The physical model of the welding process

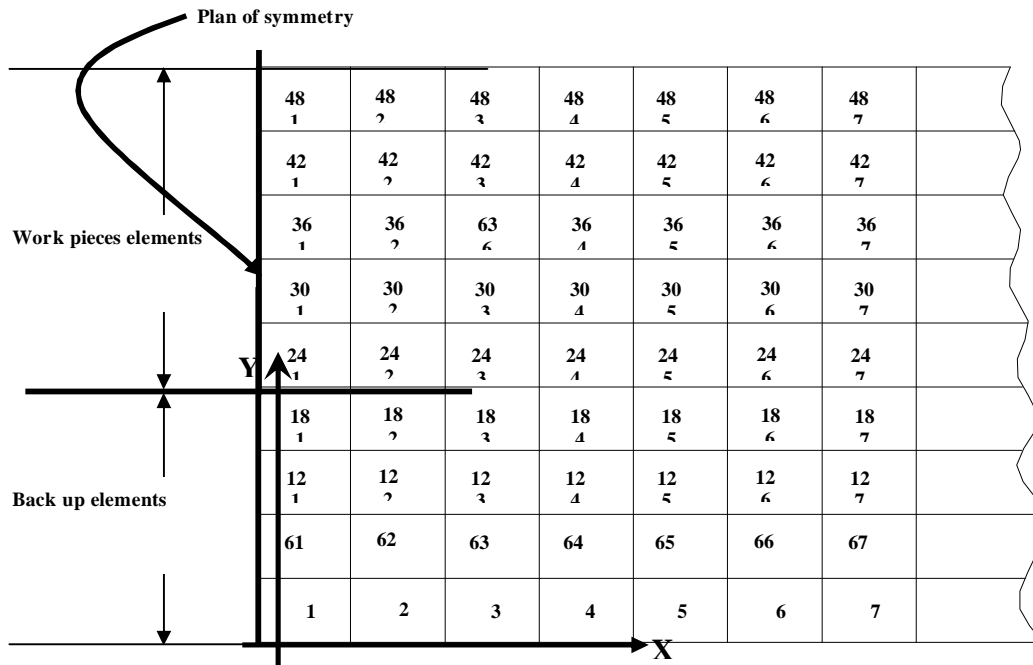


Figure (2) Dividing the Physical Domain into Elements

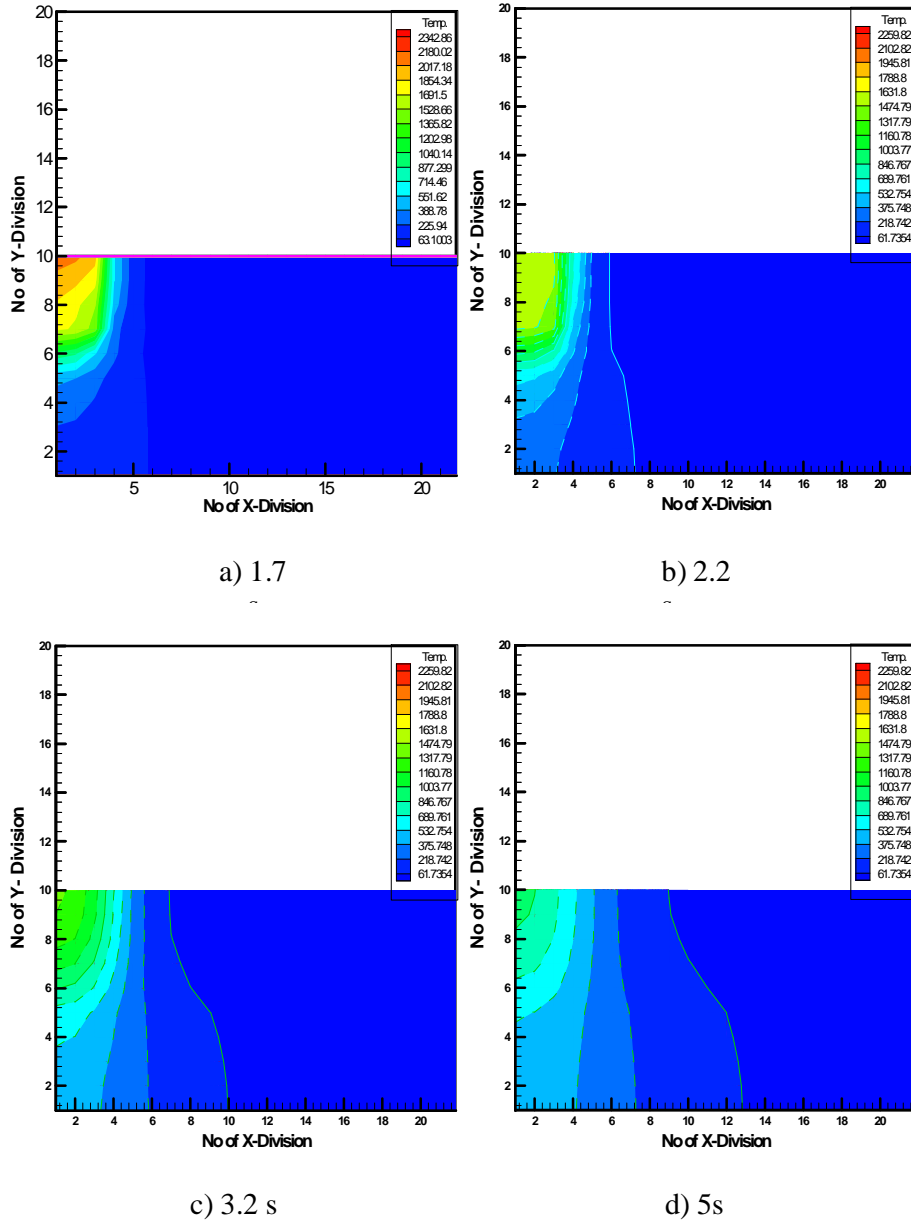


Figure (3) Temperature Distribution of Welding Current (80A) 2.5mm Case One

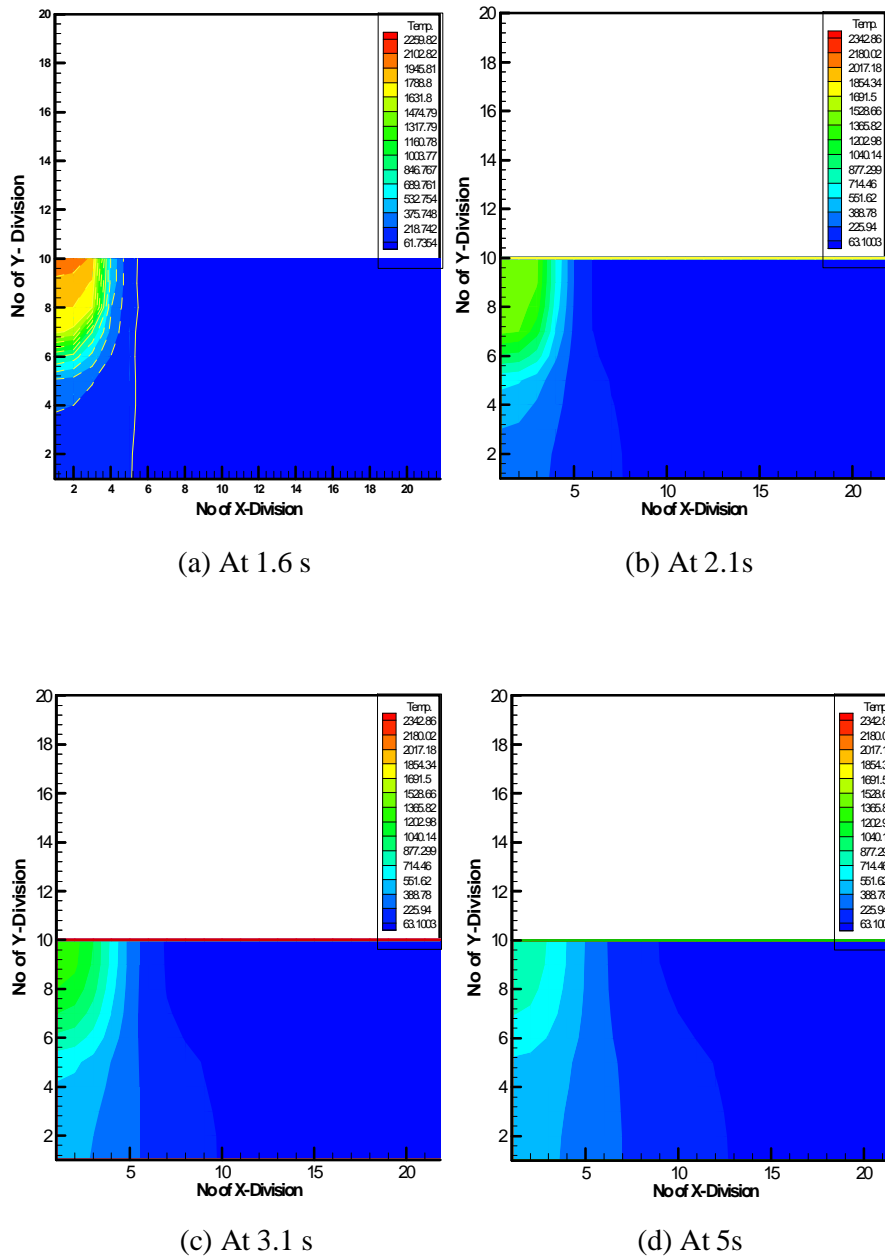


Figure (4) Temperature Distribution of Welding Current (90A) 2.5mm Case One

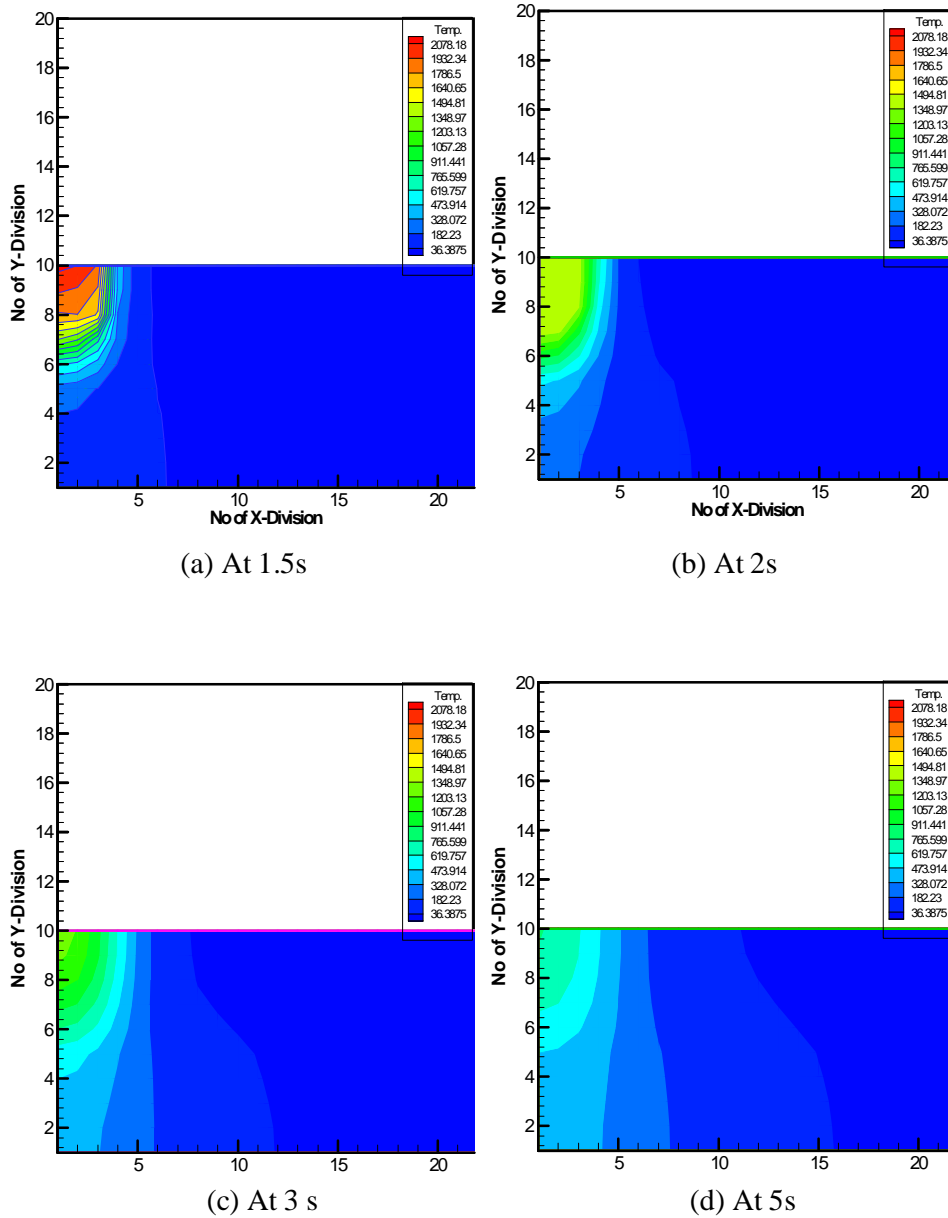


Figure (5) Temperature Distribution of Welding Current (100A)
2.5mm Case One

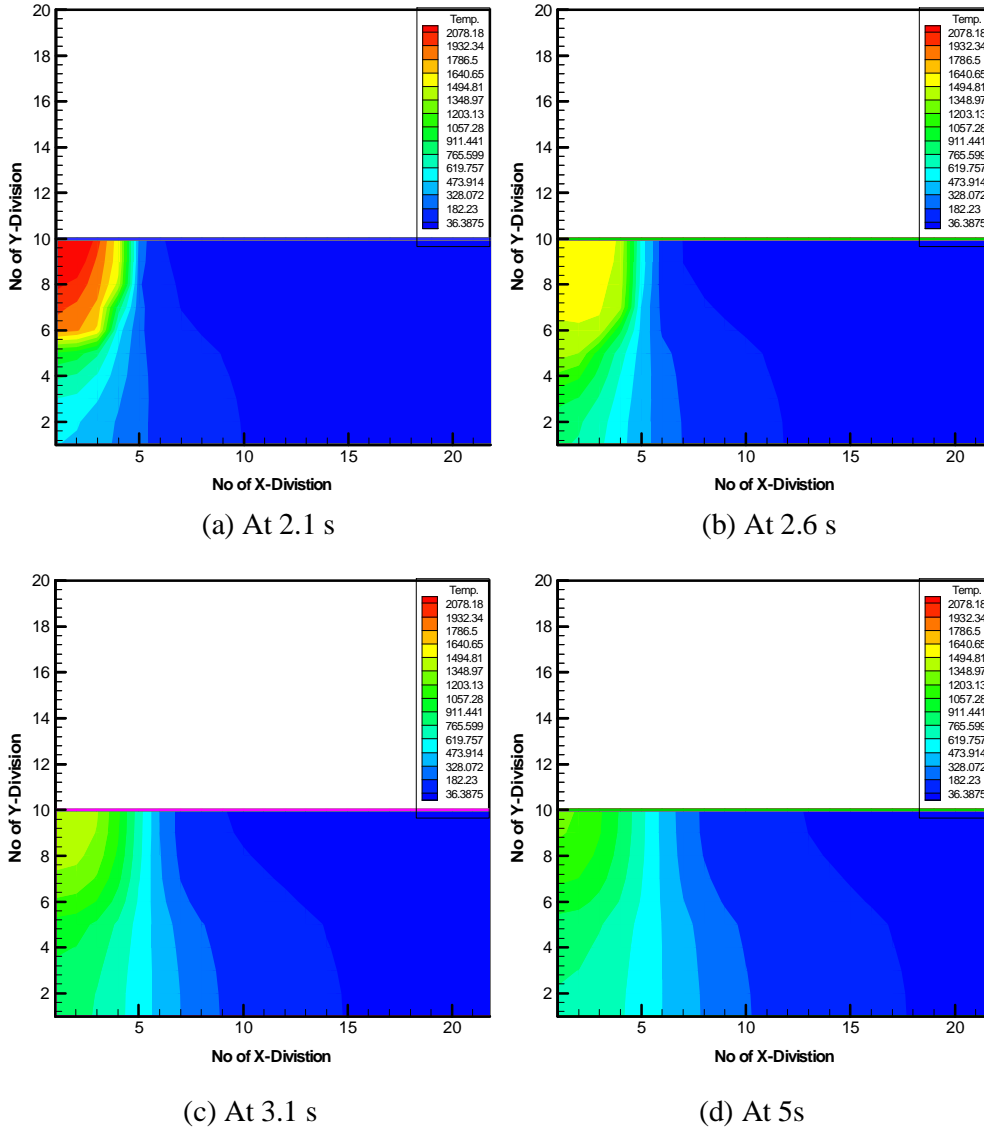


Figure (6) Temperature Distribution of Welding Current (130A) 5mm
Case Two

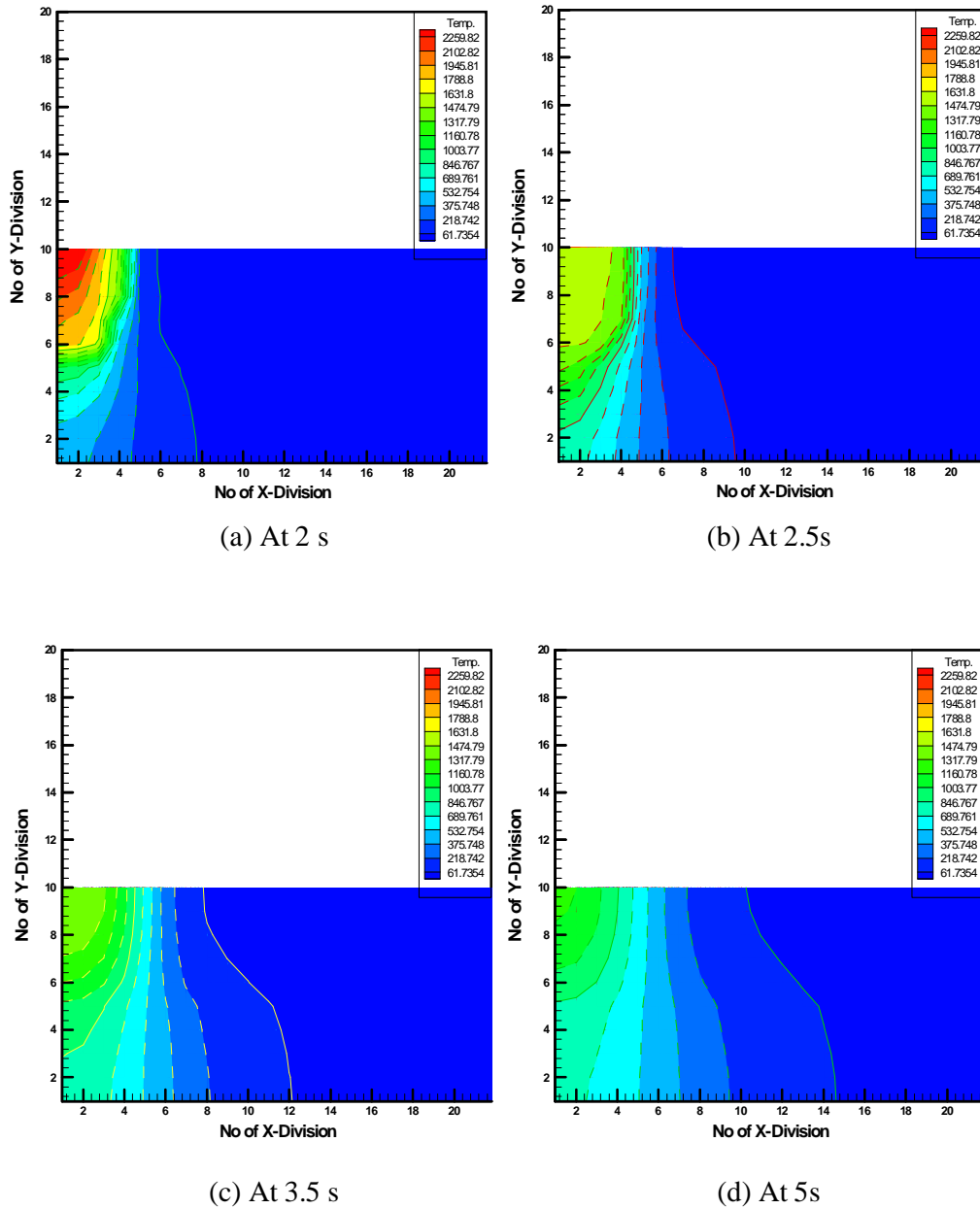
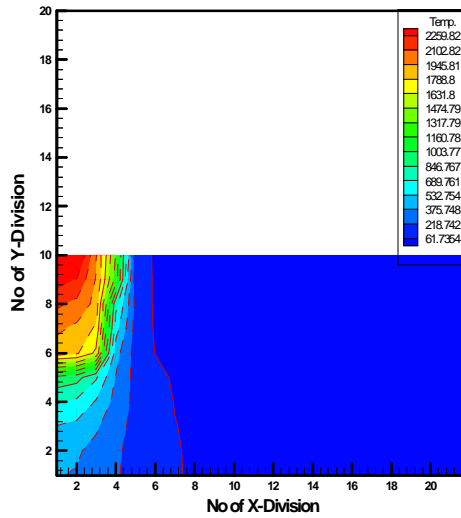
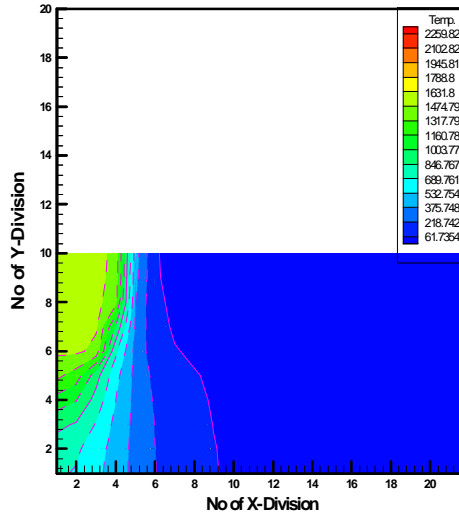


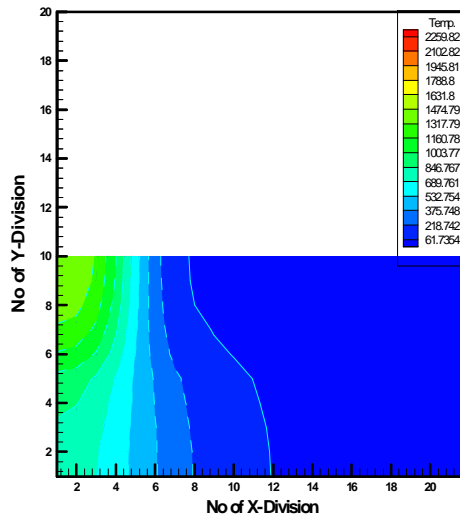
Figure (7) Temperature Distribution of Welding Current (140A) 5mm
Case Two



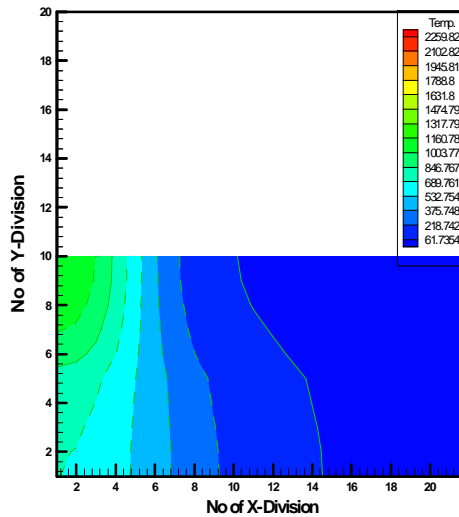
(a) At 1.9 s



(b) At 2.4s



(c) At 3.4 s



(d) At 5s

Figure (8) Temperature Distribution of Welding Current (150A)
5mm Case Two

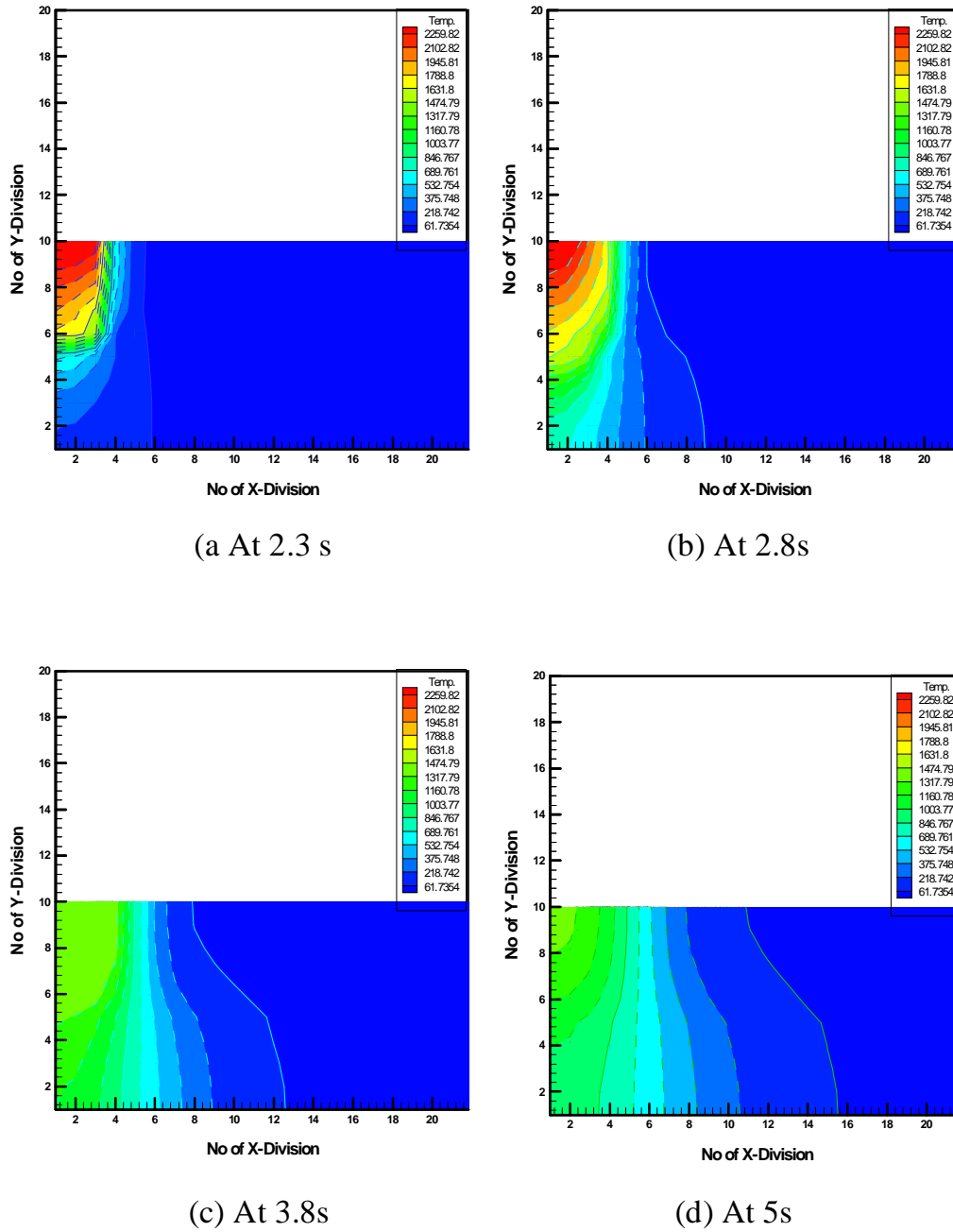


Figure (9) Temperature Distribution of Welding Current (130A) 5mm Case Three

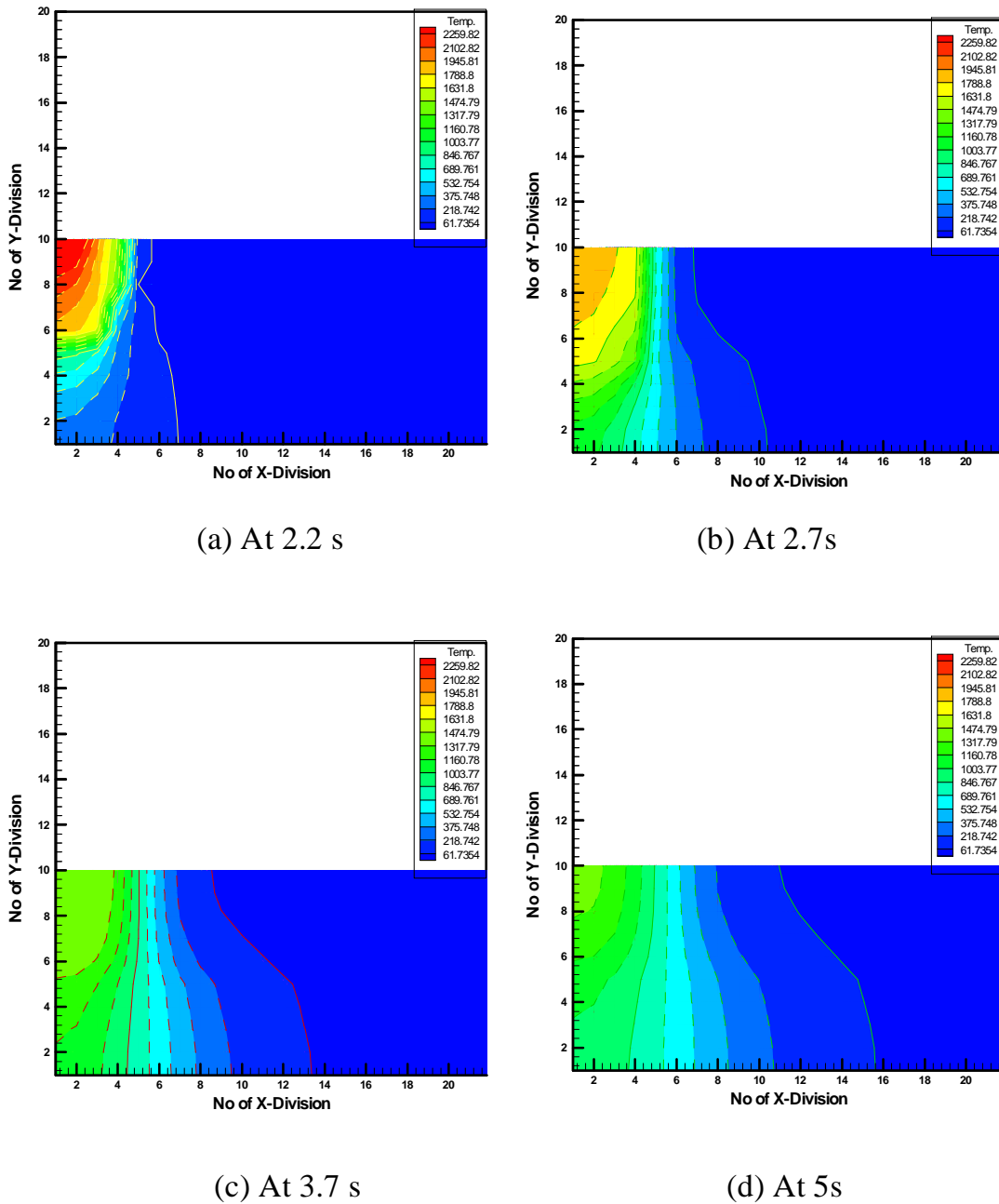
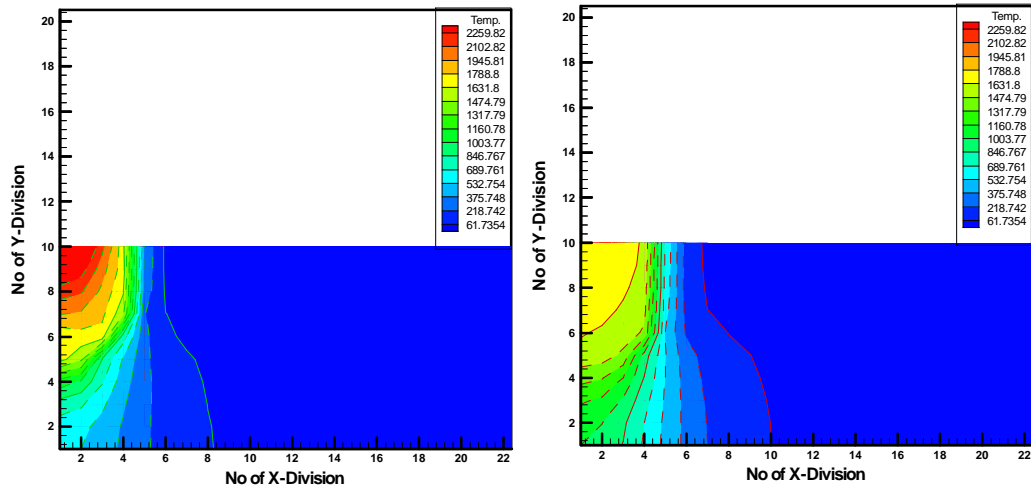
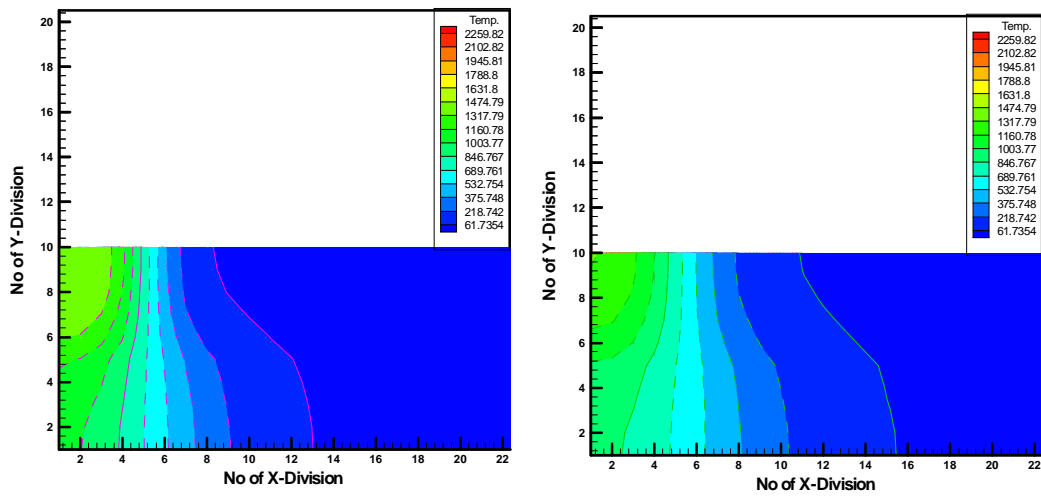


Figure (10) Temperature Distribution of Welding Current (140A) 5mm
Case Three



(a) At 2.1 s

(b) At 2.6s



(c) At 3.6 s

(d) At 5s

Figure (11) Temperature Distribution of Welding Current (150A) 5mm
Case Three

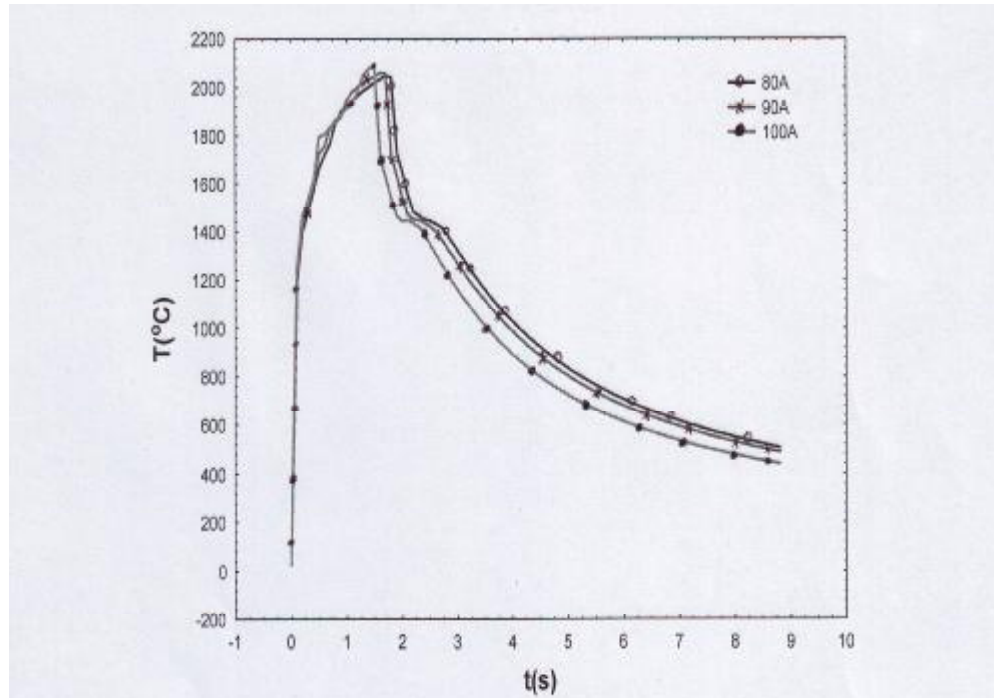


Figure (12): Temperature History Of Joint Surface at plane of Symmetry for Case (1)

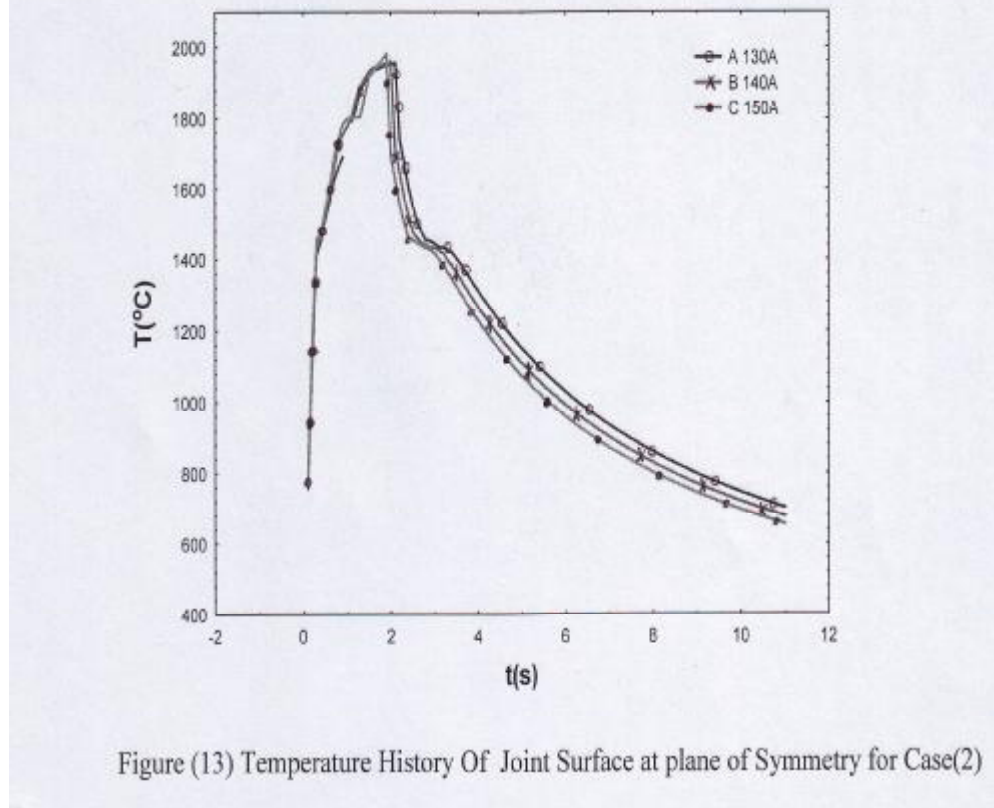


Figure (13) Temperature History Of Joint Surface at plane of Symmetry for Case(2)

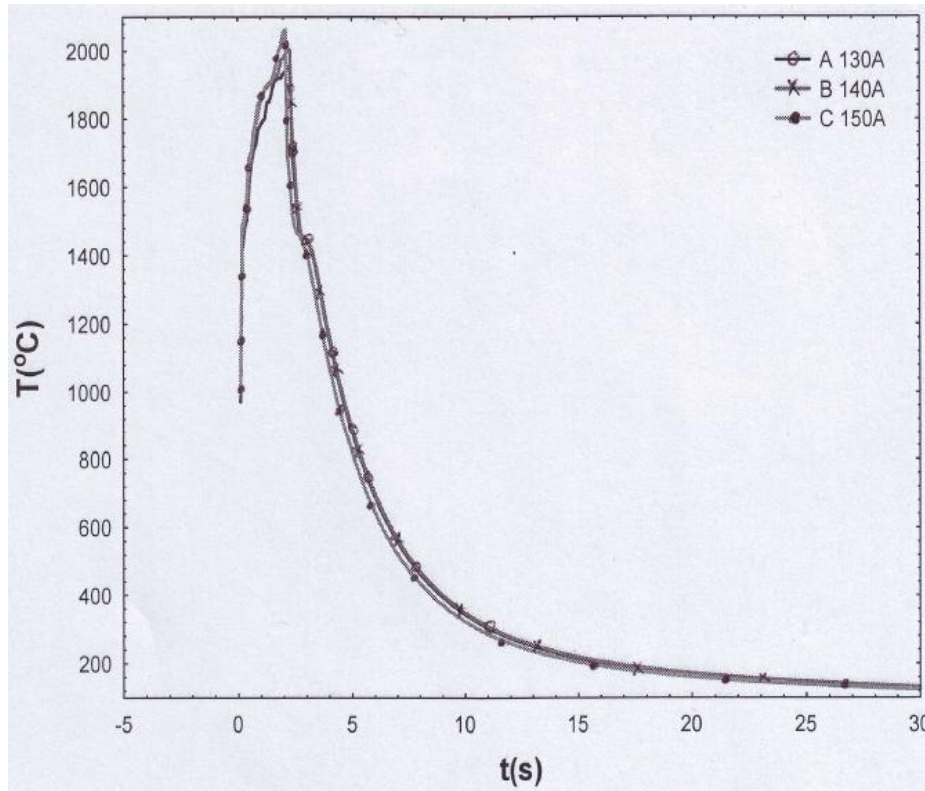


Figure (14) Temperature History Of Joint Surface at plane of Symmetry for Case (3)

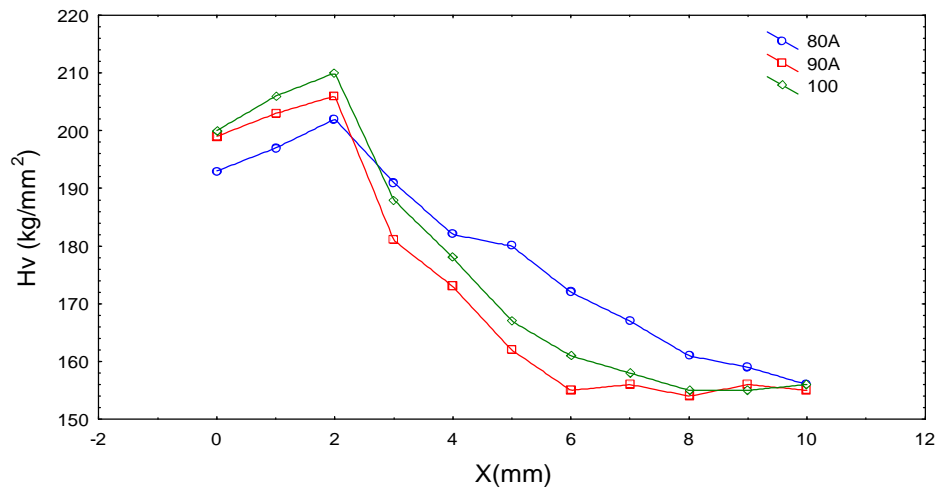


Figure (15) Microhardness of Case One (2.5mm)

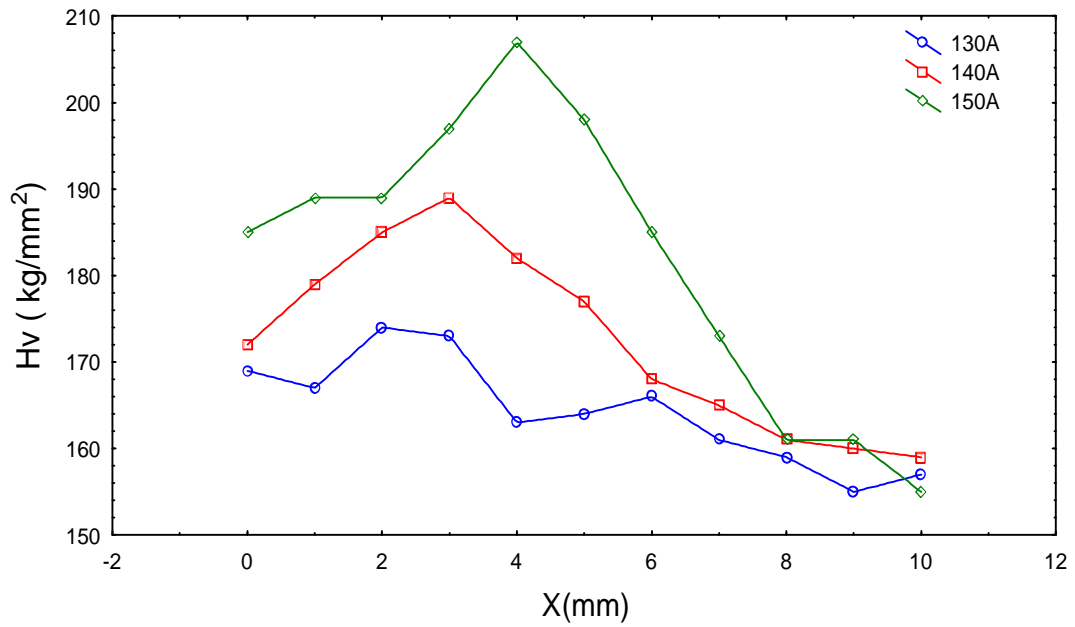


Figure (16) Microhardness of Case Two (5mm)

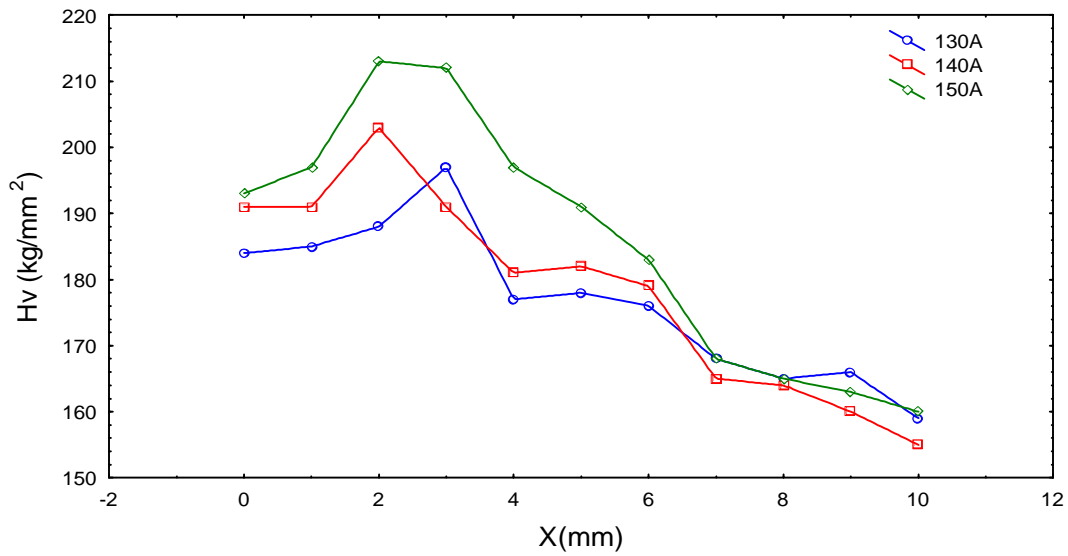
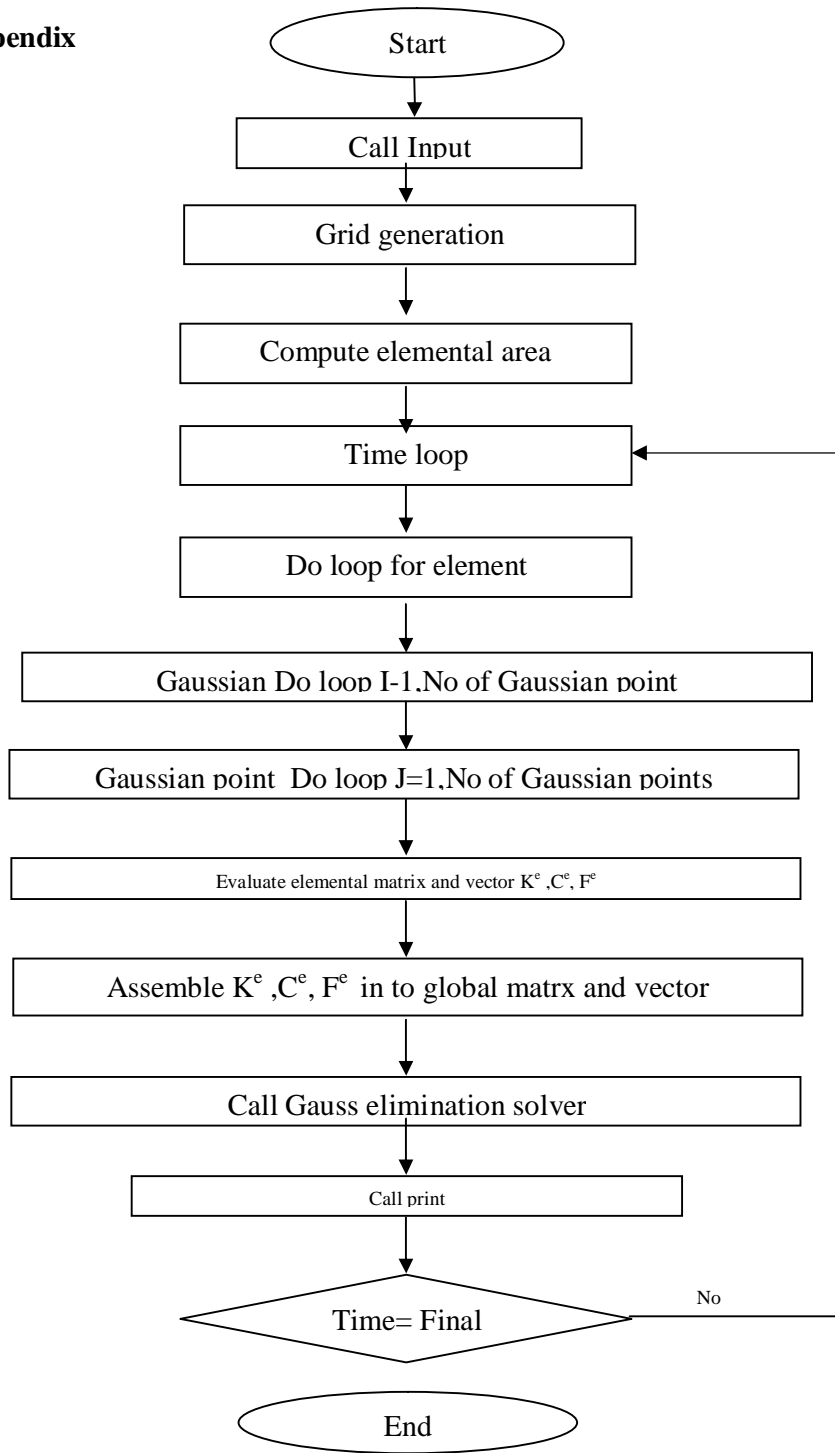


Figure (17) Microhardness of Case Three (5mm)

Appendix



Computer Program Flow Chart